Materials Research Express

**PAPER**

# Disintegration mechanism of second phase particles under electron beams

IOP Publishing    Mater. Res. Express 6 (2019) 106556    https://doi.org/10.1088/2053-1591/ab39b3

Materials Research Express

CrossMark

RECEIVED
11 May 2019

REVISED
25 July 2019

ACCEPTED FOR PUBLICATION
8 August 2019

PUBLISHED
21 August 2019

PAPER

# Disintegration mechanism of second phase particles under electron beams

**Vladimir Sarychev**[1], **Sergey Nevskii**[1], **Sergey Konovalov**[2,3], **Alexey Granovskii**[1] **and Victor Gromov**[1]

[1] Department of Natural Science, Siberian State Industrial University, Kirov street 42, 654007, Novokuznetsk, Russia
[2] Department of Materials Technology and Aviation Material Science, Samara National Research University, Moskovskoye Shosse 34, 443086, Samara, Russia
[3] Institute of Laser and Optoelectronic Intelligent Manufacturing, Wenzhou University, No. 19 Binhai 3rd Road, Yongxing Street, Wenzhou, 325024, People's Republic of China

**E-mail:** ksv@ssau.ru

**Keywords:** electron beam, zone of thermal effect, silumin, silicon, aluminum, Rayleigh-Taylor instability

## Abstract

The paper suggests a disintegration mechanism of silicon particles in aluminum in the heat-impact zone of a low-energy high-current electron beam. This inclusion was modeled with a round plate (radius R and thickness h). Disintegration of silicon inclusion was assumed to be possible due to discrepancy of elasticity modulus and linear expansion thermal coefficient caused by the evolving dynamic instability. In conditions of high-speed cooling a silicon plate is subjected to compression stresses, since linear expansion coefficient of aluminum is above that of silicon. If these forces applied, instability and fracture of a plate are registered. Using methods of elasticity theory it was found out that the value of these stresses is around 1 GPa. The initial stage of this instability was analyzed by methods of Theory of Plates and Shells. In terms of this theory, a critical stress ($\sim 10^7$–$10^9$ Pa) was determined close to the clamped ends of a plate and hinged plates. So, it was concluded, that a suggested mechanism of silicon particles disintegration in the heat-impact zone of an electron beam seems to be the most probable one. Relay-Taylor instability on the inclusion and matrix border is thought to be another mechanism of particles disintegration. According to the linear analysis of this instability, a wavelength with the maximal growth speed of disturbances is $\sim 4$ $\mu$m, for inclusions $\sim 1$ $\mu$m these findings exceed significantly the experimental data.

## 1. Introduction

Aluminum—silicon alloys (silumins) are widely applied in aircraft production, motor-car manufacturing, and other industries. Satisfactory casting properties make possible to use them for manufacturing thin-wall and water-proof foundry goods with complex physical configuration. A shortcoming of silumins is low mechanical properties because of rough dispersive inclusions of silicon. These inclusions are concentrators of mechanical stresses, a high level of which causes cracking. Therefore, it's necessary to develop methods of reducing the sizes of silicon inclusions. To date, different types of heat treatment have been used in order to find a solution of this problem, including application of concentrated energy flows (laser treatment, electron-beam-treatment etc) [1–8]. In the process of heat treatment of multiphase alloys particles of the second phase are subject to two types of transformations: (1) coalescence, i.e. enlargement of these particles; (2) refinement of the second phase particles with the subsequent spheroidization. The second transformation is considered in more details. Studies [7, 8] have revealed that this process is based on the mechanism of diffusion due to the gradient of concentration on the border ≪second phase/matrix≫. This process accelerates as the temperature rises. Second phase inclusions can have an equiaxed configuration, since plates or needles split into several particles. Crystal lattice defects in the matrix and second phase are important for splitting. Studies [9, 10] demonstrate that second phase particles with an equiaxed configuration are formed due to the surface tension and suggest a simple dynamic model of this process. Grinfeld [11, 12] analyzed a second variation of available energy function in the system

≪melt/crystal≫ and found out, that non-hydrostatic components of a stress field in the elastic crystals cause instability of their interface, furthermore, the development of this instability results from dissolving a solid phase by liquid or transport of particles on crystal edge. The interphase surface tension can't damp this instability in a long-wavelength range; however, it has a stabilizing effect. This instability develops if both phases are solids. It develops mainly because shift stresses exceed slightly their critical value, which, in its turn, is dominated by the ratio of longitudinal and transverse speed of sound.

The study [13] provided a deep insight into the behavior of perlite structure when pulse loading. It indicated fragmentation of perlite components into ultrathin particles at the beginning of high-speed stretching (in the zone of unloading wave interference). Cement carbide as an instable phase starts dissolving, and carbon gets into a reaction with ferrite, new globules of cement carbide are found on some spots on the interface of ferrite and cement carbide. The second stage in mechanical-chemical spheroidization of perlite is possible due to additional introduction of carbon atoms from matrix into the spall damaging zone. Ultrathin dimensions of particles, dissolution of perlite components and their saturation with carbon in the second chemical reaction results probably in the increase of cementite concentration due to the substitution reaction between additional carbon and iron. Similar mechanism was found in differently hardened rail steel operated for a long time [14, 15]. Studies [16, 17] analyzed dissolution of carbon particles under electron beams, according to their findings, a principal mechanism of dissolution is diffusion, inclusion thickness versus time ratio was determined. Researchers found that nano-dimensional particles dissolve quicker than micro-dimensional ones. Diffusion coefficient of silicon in aluminum is around $10^{-16}$ cm$^2$ s$^{-1}$ for silumins, therefore, dissolution time of inclusions ranges ~10–100 s, so diffusion isn't a main mechanism of disintegration and spheroidization in aluminum and silicon alloys treated by electron beams. Study [18] highlighted a mechanism, which says that destruction of silicon plates leads to spheroidization because linear expansion thermal coefficients of matrix and inclusion are different. For instance, the share of silicon plates is much smaller than that of aluminum matrix, so it is aluminum matrix that has the biggest effect on thermal expansion. Linear expansion coefficient of aluminum is 4 times higher than that of silicon. Therefore, thermal expansion (compression) of two phases is mutually exclusive. As a consequence, mechanical stresses arise inevitably between phases. Inclusions of silicon can absorb only a quarter (¼) of thermal expansion (compression) emitted by aluminum matrix through its own thermal expansion (compression). The remaining part is important for matrix deformation and destruction of silicon plates (due to their brittleness). Non-homogenous surface of inclusion causes cracking. Cracks are capillary vessels for aluminum atoms. Mechanical stresses created by cracks are analogues of capillary forces, which move atoms of matrix into the gaps formed between inclusions. Flows of vacancies and silicon atoms have a reverse direction. A similar mechanism of second phase particles disintegration has been found in conditions of pulse high-density electric current impact [19] and selective laser melting [20]. Researchers [21, 22] investigated instability of the interface between materials under contact loading. Linear analysis revealed two instabilities, which differ significantly from a wave-guiding instability: (1) dynamical instability, initiated by modes, propagating as fast as a dilatation wave contrarily to the sliding movement with a low wavenumber; (2) dynamical instability, arising due to modes propagating as fast as shear waves toward sliding.

To sum up, both disintegration mechanisms despite being different result in instability in the surface of the second phase coarse inclusion.

Figure 1(a) gives electronic-microscopic image of silumin structure in the initial state.

As seen in the figure, silumin is a multiphase aggregate, made up by aluminum-based solid solution grains, eutectic Al-Si grains, primary silicon inclusions, and intermetallic compounds, shape and dimensions of which are quite different. Electron beam treatment results in formation of a multi-layer gradient structure. In morphology of the defect sub-structure three layers are identified, in this study [24] they are referred to as surface, intermediate and thermal impact layer. The surface layer has a columnar crystallization structure, which is formed when high-speed cooling of molten material (figure 1(b)). According to SEM-data thickness of this layer ranges 70 to 100 $\mu$m. TEM-based analysis of the intermediate layer [23] revealed primary inclusions of the second phase in its structure (figure 1(c)), which are centers of aluminum crystallization. Dimensionally these inclusions are shown in figure 2. This regularity has a bimodal character. Particles are 138.9 ± 45.3 nm on average. So, decrement of disturbances on the interface is assumed to have two maximums.

## 2. Problem formulation

A mechanism of silicon plate disintegration is assumed to evolve in the heat-impact zone under electron-beam treatment. A silicon plate incorporated in aluminum matrix is analyzed. As mentioned in Introduction, different elasticity modules and linear expansion coefficients of aluminum and silicon on the interface of inclusion and matrix are the reason for mechanical stresses, which cause its instability and fracture. Figure 3 shows a silicon plate contacts with aluminum matrix at the stage of cooling. At this point a plate of silicon is loaded with

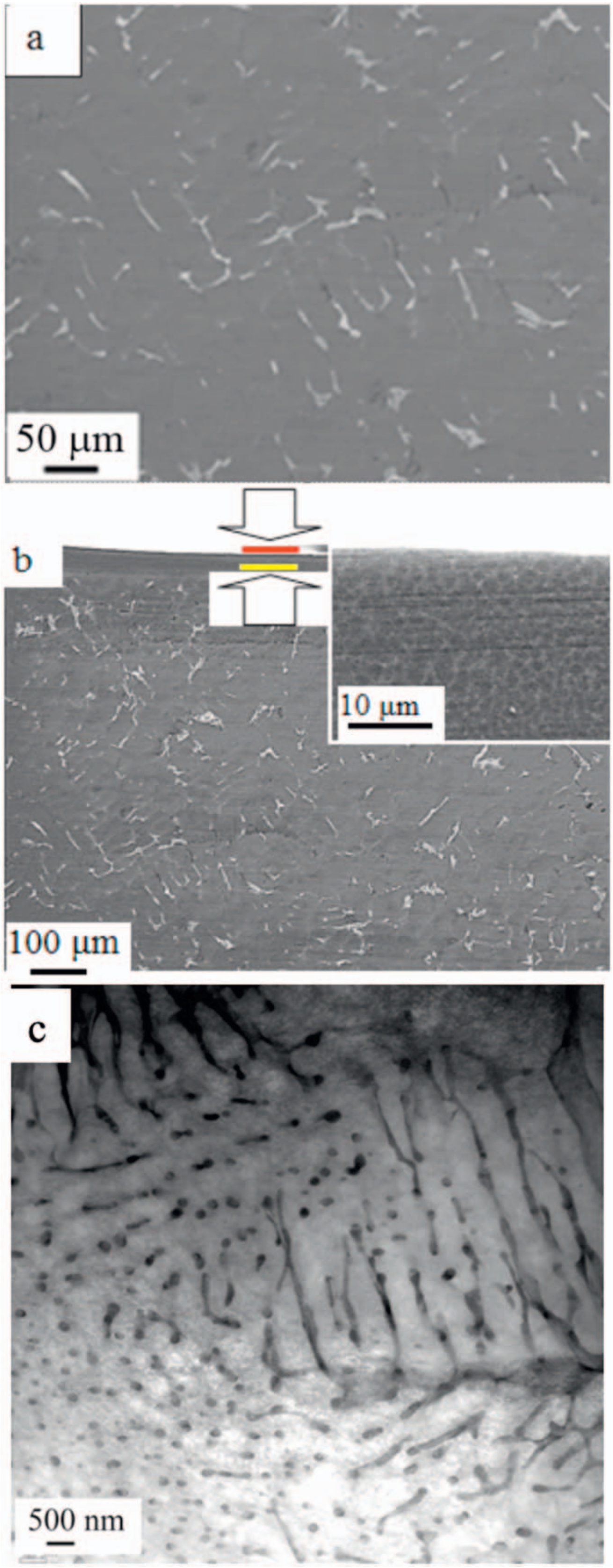


**Figure 1.** Structure of silumin: (a) initial state; (b) and (c) irradiated by a pulse electron beam with energy density 35 J $cm^{-2}$ [23].

compressive stresses [18]. A shape of inclusion is approximated to a round and principles of theory of elastic stability are applied [24–27]. Following these assumptions, two cases are considered: (1) silicon inclusion is a hinged plate on all sides; (2) plate is clamped on all sides. A force $P$ is applied to the plate along radius in all cases.

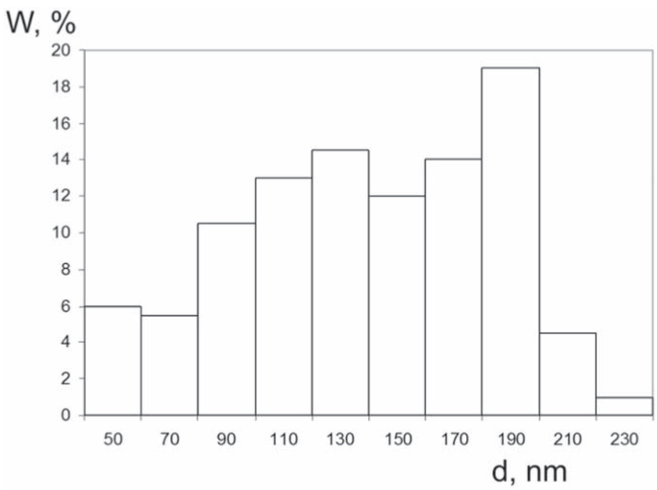


**Figure 2.** Size distribution of silicon particles in the heat-impact zone [23].

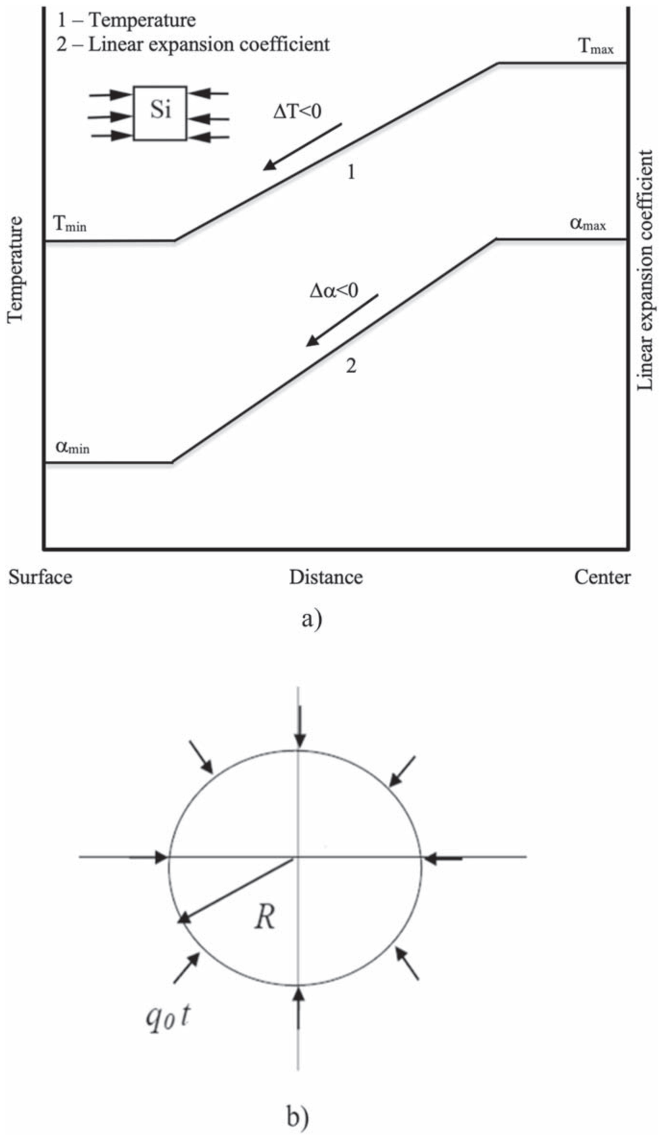


**Figure 3.** A principle of a silicon plate contact with aluminum matrix: (a) temperature (curve 1) and linear expansion coefficient (curve 2) changing at the stage of cooling; (b) principle of loading a silicon plate.

A stress-strain problem close to the inclusion is to be solved to determine this force. For this purpose a system of differential equations is written according to radial movement (u(r)), elasticity modulus (E), Poisson ratio ($\nu$), and linear expansion coefficient ($\alpha$) are constant:

$$\frac{d}{dr}\left(\frac{1}{r}\frac{dru_n}{dr}\right) = (1+\nu_n)\alpha_n\frac{dT_n}{dr}. \tag{1}$$

The first layer is in the range $0 < r < a$ with parameters of material $E_1,\ \nu_1,\ \alpha_1$, the second one —$a < r < \infty$ and $E_2,\ \nu_2,\ \alpha_2$, where $E_n,\ \nu_n,\ \alpha_n$– elasticity modulus, Poisson coefficient and linear expansion coefficient, respectively. External boundary conditions at $r = 0$ и $r \to \infty$:

$$u_1(0) = 0,\ u_2(\infty) = 0. \tag{2}$$

A solution, meeting external boundary conditions is as follows:

$$u_1(r) = (1+\nu_1)\frac{\alpha_1}{r}\int_0^r T_1(\xi)\xi d\xi + C_1 r$$
$$u_2(r) = (1+\nu_2)\frac{\alpha_2}{r}\int_a^r T_2(\xi)\xi d\xi + \frac{C_2}{r}. \tag{3}$$

Components of stresses

$$\sigma_{r1}(r) = -\frac{\alpha_1 E_1}{r^2}\int_0^r T_1(\xi)\xi d\xi + C_1\frac{E_1}{1-\nu_1},$$
$$\sigma_{r2}(r) = -\frac{\alpha_2 E_2}{r^2}\int_a^r T_2(\xi)\xi d\xi - C_2\frac{E_2}{r^2(1+\nu_2)}. \tag{4}$$

Matching conditions of layers are written as a congruence of radial stresses and movement in the point of layer contact $r = a$:

$$-E_1\Phi + C_1\frac{E_1}{1-\nu_1} = -C_2\frac{E_2}{a^2(1+\nu_2)},$$
$$(1+\nu_1)a\Phi + C_1 a = \frac{C_2}{a};$$
$$\Phi = \frac{\alpha_1}{a^2}\int_0^a T_1(\xi)\xi d\xi \tag{5}$$

The solution of system (5)

$$C_1 = \left(\frac{1-K}{1+K} - \nu_1(1+K)\right)\Phi,$$
$$C_2 = \frac{2a^2\Phi}{1+K};\ K = \frac{E_2(1-\nu_1)}{E_1(1+\nu_2)}. \tag{6}$$

Distribution of temperatures is to be calculated in order to determine stresses. We address to the case of a constant temperature, so

$$\Phi = \frac{\alpha_1}{2}T_0 \tag{7}$$

Taking into account (6) and (7), stresses on the boundary are written as follows:

$$\sigma_1 = \frac{B_1 B_2(1+\nu_1)T_0((\alpha_1-\alpha_2)\nu_2 - (\alpha_1+\alpha_2))}{B_1\nu_1 - B_2\nu_2 + B_1 + B_2} \tag{8}$$

where $B_1 = \dfrac{E_1}{1-\nu_1},\quad B_2 = \dfrac{E_2}{1-\nu_2}$

Having found the distribution of stresses along the inclusion radius, its stability is to be focused on. The main motion equation [26, 27] in terms of Theory of Plates and Shells is written as follows:

$$D\Delta\Delta w + P\Delta w + \rho h\frac{\partial^2 w}{\partial t^2} = 0 \tag{9}$$

where w—transverse displacement, P—load, $\rho$—density of the plate material, $h$—its thickness, $D = \dfrac{Eh^3}{12(1-\nu^2)}$ – bending stiffness, $\Delta$ – Laplace operator in polar coordinates. The solution is searched as given below (9)

$$w(r,\ \varphi,\ t) = Z(t)w_{mn}(r)\cos n\varphi \tag{10}$$

where Z(t) and $w_{mn}(r)\cos(n\varphi)$ – temporal and coordinate components of transversal displacement. The amplitude of this displacement $w_{mn}(r)$ is dominated by boundary conditions. For hinged plates boundary conditions are written as follows in equation (9):

$$\frac{d^2 w_{mn}}{dr^2} + \frac{\nu}{r}\frac{dw_{mn}}{dr} = 0 \text{ at } r = R, \tag{11}$$

and for clamped ones:

$$w_{mn} = \frac{dw_{mn}}{dr} = 0 \text{ at } r = R. \tag{12}$$

Initial conditions are written:

$$Z(0) = 0, \quad \dot{Z}(0) = 0 \tag{13}$$

The criterion of instability suggested in [28] is used:

$$\dot{Z}(t_{cr}) = 0 \tag{14}$$

where $t_{cr}$ – critical time (moment of instability initiation).

## 3. Results and discussion

To solve the problem (9)–(14) Bubnov-Galerkin method is applied. The internal load is as $P = q_0 t$, where $q_0$ – rate of loading. For a hinged plate the coordinate component of its displacement is stated as:

$$w_{mn}(r) = J_n(\beta_{n,m}R)\left(\frac{r}{R} - \left(\frac{r}{R}\right)^n\right) \tag{15}$$

where $\beta_{n,m}$ – equation root:

$$(\beta_{n,m}R)J_n(\beta_{n,m}R) - (1 - \nu)J_{n+1}(\beta_{n,m}R) = 0 \tag{16}$$

where $J_n(\beta_{n,m}R)$ – Bessel function of n-order. The critical load $P_{cr} = q_0 t_{cr}$ is written as follows in this case:

$$q_0 t_{cr} = \beta_{m,n}^2 \frac{D}{R^2} + \frac{b_1 \rho h R^2}{\beta_{m,n}^2 t_{cr}^2}\frac{(\beta_{m,n}^2 - 2(1 + \nu^2))}{\beta_{m,n}^2 - 1 - \nu^2} \tag{17}$$

For a clamped plate $w_{mn}(r)$

$$w_{mn}(r) = J_n(\alpha_{n+1,m}R)\left(\frac{r}{R} - \left(\frac{r}{R}\right)^n\right) \tag{18}$$

where $\alpha_{n+1,m}$ – equation root:

$$J_{n+1}(\alpha_{n+1,m}R) = 0 \tag{19}$$

The critical load $P_{cr} = q_0 t_{cr}$ for a clamped plate is:

$$q_0 t_{cr} = \alpha_{m,n}^2 \frac{D}{R^2 h} + \frac{b_1 \rho R^2}{\alpha_{m,n}^2 t_{cr}^2} \tag{20}$$

The critical load for static loading of a hinged plate is written:

$$p_{cr} = \beta_{m,n}^2 \frac{D}{R^2 h} \tag{21}$$

and for a clamped plate:

$$p_{cr} = \alpha_{m,n}^2 \frac{D}{R^2 h} \tag{22}$$

For complex roots $\alpha_{m,n} = \frac{\pi}{4}(2m + 4n + 1)$, $\beta_{m,n} = \pi\left(2n + m + \frac{3}{4}\right)$. Table 1 provides input data for calculations.

As found in (21) and (22), critical loads for inclusions with a radius R $\sim$ 10 $\mu$m and thickness h $\sim$ 1 $\mu$m are $p_{cr} \approx 4.22 \cdot 10^8$ Pa, $p_{cr} \approx 1.48 \cdot 10^9$ Pa. The stress on the interface of the inclusion is 1.19 GPa at temperature 577 K according to data in (8). For inclusions with thickness h ~100 nm critical loads are for the first case – $p_{cr} \approx 4.25 \cdot 10^6$ Pa, and for the second – $p_{cr} \approx 1.49 \cdot 10^7$ Pa. For inclusions with a radius R˜ 100 $\mu$m and thickness h ~1 $\mu$m it is in the first case $p_{cr} \approx 7.51 \cdot 10^7$ Pa, and in the second .. Pa.

Therefore, we can conclude that a suggested mechanism provides a reasonable explanation of silicon plate disintegration in the heat-impact zone in electron-beam treatment. Another mechanism of silicon plate

**Table 1.** Material characteristics of matrix and inclusion.

| Characteristic | Material | |
|---|---|---|
| | Al | Si |
| Elasticity modulus, GPa | 70 | 110 |
| Linear expansion coefficient, $K^{-1}$ | $28.1 \cdot 10^{-6}$ | $3.68 \cdot 10^{-6}$ |
| Poisson coefficient | 0.3 | 0.3 |

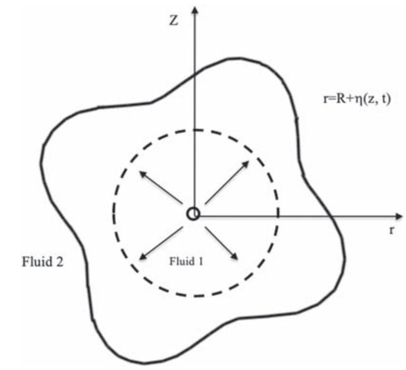


**Figure 4.** Principle of Relay-Taylor instability initiation in geometry of cylindrical bodies.

disintegration is Relay-Taylor instability on the interface ≪inclusion/matrix≫. Mechanical stresses are mass forces in this case; these stresses arise, as mentioned above, due to different elasticity modules and liner expansion thermal coefficients. Studies [28, 29] were focused on the initial stage of this instability in geometry of cylindrical bodies. Figure 4 demonstrates initiation of this instability. Dimensions of particles formed are proportional to a wavelength with the maximal growth rate of disturbances on the interface. A dispersion equation is to be solved to determine this wavelength.

Study [29] suggested a dispersion equation for the simple case of viscous-potential flow with consideration of viscosity on the interface only. Applying this approach to the case under consideration, a motion equation and boundary conditions are written as follows:

$$\begin{gathered}\frac{\partial u_1}{\partial r} + \frac{u_1}{r} + \frac{\partial w_1}{\partial r} = 0,\ \frac{\partial u_1}{\partial t} + \frac{\partial p_1}{\rho_1 \partial r} = 0,\ \frac{\partial w_1}{\partial t} + \frac{\partial p_1}{\rho_1 \partial z} = 0;\\ \frac{\partial u_2}{\partial r} + \frac{u_2}{r} + \frac{\partial w_2}{\partial r} = 0,\ \frac{\partial u_2}{\partial t} + \frac{\partial p_2}{\rho_2 \partial r} = 0,\ \frac{\partial w_2}{\partial t} + \frac{\partial p_2}{\rho_2 \partial z} = 0\end{gathered} \tag{23}$$

Kinematic conditions on the interface $r = R + \eta(t, z)$:

$$\frac{\partial \eta}{\partial t} = u_1,\ \frac{\partial \eta}{\partial t} = u_2. \tag{24}$$

Dynamic boundary conditions:

$$\begin{gathered}p_2 - p_1 + 2\rho_1 \nu_1 \frac{\partial u_1}{\partial r} - 2\rho_2 \nu_2 \frac{\partial u_2}{\partial r} =\\ = \sigma\left(\frac{\eta}{R^2} + \frac{\partial^2 \eta}{\partial z^2}\right) - (\rho_2 - \rho_1) g \eta(x,\ t).\end{gathered} \tag{25}$$

Impermeability conditions are set on external boundaries:

$$u_1(R_1) = 0, \quad u_2(R_2) = 0 \tag{26}$$

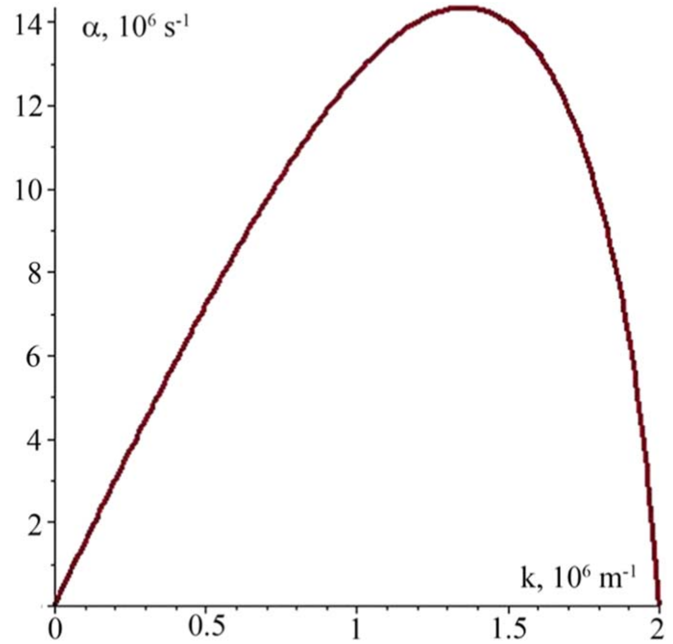


**Figure 5.** Decrement of disturbance versus wavenumber.

**Table 2.** Data for calculating growth rate of disturbances.

| Parameter | Material | |
|---|---|---|
| | Al | Si |
| Density, kg/m$^3$ | 2700 | 2330 |
| Kinematic viscosity, m$^2$/s | $1.4 \cdot 10^{-6}$ | $\sim 10^{-6}$ |
| Surface tension, N/m$^2$ | 1.14 | 1.67 |

The solution (23)–(27) is searched:

$$u_1(r, z, t) = U_1(r)\exp(\omega t + ikz),$$
$$u_2(r, z, t) = U_2(r)\exp(\omega t + ikz),$$
$$p_1(r, z, t) = P_1(r)\exp(\omega t + ikz),$$
$$p_2(r, z, t) = P_2(r)\exp(\omega t + ikz),$$
$$\eta(z, t) = \eta_0 \exp(\omega t + ikz). \tag{27}$$

Substituting (27) into (23)–(26), a dispersion equation is written

$$\omega^2 + a\omega + c = 0 \tag{28}$$

where $a = \left(\frac{2k^2(E_1 - 1)\nu_1}{E_1 - E_2\theta} - \frac{2k^2\theta(E_2 - 1)\nu_2}{E_1 - E_2\theta}\right)$, $c = \frac{(x^2 - 1)\omega_c^2}{x(E_1 - E_2\theta)} - \frac{x^2(\theta - 1)g}{(E_1 - E_2\theta)R}$, $E_1 = x\frac{K_1(x_1)I_0(x) + K_0(x)I_1(x_1)}{K_1(x)I_1(x_1) - K_1(x_1)I_1(x)}$, $E_2 = -x\frac{K_1(x_2)I_0(x) + K_0(x)I_1(x_2)}{K_1(x)I_1(x_2) - K_1(x_2)I_1(x)}$.

The acceleration of layers is estimated as a relation of thermo-elastic stresses to the difference in layer densities multiplied by amplitude of disturbances: $g = \frac{1}{(\rho_1 - \rho_2)\eta_0}\left(\frac{E_1\alpha_1 T_0}{1 - 2\nu_1} - \frac{E_2\alpha_2 T_0}{1 - 2\nu_2}\right)$. Acceleration for amplitude of disturbances of 1 $\mu$m is around $10^{12}$ m s$^{-2}$.

The solution (28) is written:

$$\omega = -\frac{a}{2} + \frac{1}{2}\sqrt{a^2 - 4c} \tag{29}$$

Instability arises if $\alpha = \mathrm{Re}(\omega) > 0$. Figure 5 shows the growth rate of disturbances on the interface versus wavenumber for an inclusion of ~1 $\mu$m. The data for calculation are provided in table 2. This figure shows that a wavenumber (wavelength) with the maximal growth rate is $\sim 1.38 \cdot 10^6$ m$^{-1}$ (4.62 $\mu$m), it exceeds significantly experimental data.

Viscous-potential approximation used in the study is relevant for inclusions up to 10 $\mu$m. For bigger diameters than 10 $\mu$m viscosity both on the interface and throughout matrix and inclusion is to be taken into consideration.

## Acknowledgments

The study is conducted under financial support of the Ministry of Science and Higher Education of the Russian Federation as a part of State Oder № 3.1283.2017/4.6 and Grant of the President to support young researchers—candidates of sciences № MK - 118.2019.2.

## ORCID iDs

Sergey Konovalov https://orcid.org/0000-0003-4809-8660
Victor Gromov https://orcid.org/0000-0002-5147-5343

## References

[1] Zheng T, Zhou B, Zhong Y, Wang J, Shuai S, Ren Z, Debray F and Beaugnon E 2019 Solute trapping in Al-Cu alloys caused by a 29 Tesla super high static magnetic field *Sci. Rep.* **9** 266
[2] Deev V B, Prusov E S and Kutsenko A I 2018 Theoretical and experimental evaluation of the effectiveness of aluminum melt treatment by physical methods *Metallurgia Italiana* **110** 16
[3] Panin S V, Vlasov I V, Sergeev V P, Ovechkin B B, Marushchak P O, Ramasubbu S, Lyubutin P S and Titkov V V 2015 Fatigue life enhancement by irradiation of 12Cr1MoV steel with a $Zr^+$ ion beam. Mesoscale deformation and fracture *Phys. Mesomech.* **18** 261
[4] Fomin A A 2017 Limiting product surface and its use in profile milling design operations *Solid State Phenomena* **265** 672
[5] Ramazanov K N, Vafin R K and Khusainov Yu G 2014 Ion nitriding of tool steel kh12 in glow discharge in cross electric and magnetic fields *Met. Sci. Heat Treat.* **56** 50
[6] Ghyngazov S A, Vasil'ev I P, Surzhikov A P, Frangulyan T S and Chernyavskii A V 2015 Ion processing of zirconium ceramics by high-power pulsed beams *Tech. Phys.* **60** 128
[7] Robles Hernandez F C, Herrera Ramírez J M and Mackay R 2017 *Al-Si Alloys : Automotive, Aeronautical, and Aerospace Applications* (Berlin: Springer) 978-331958380-8;978-331958379-2 (https://doi.org/10.1007/978-3-319-58380-8)
[8] Nafisi S and Ghomashchi R 2016 *Semi-Solid Processing of Aluminum Alloys* (Berlin: Springer) (https://doi.org/10.1007/978-3-319-40335-9)
[9] Stuwe H P and Kolednik O 1988 Shape instability of thin cylinders *Acta Metall.* **36** 1705
[10] Ogris E, Wahlen A, Luchinger H and Uggowitzer P J 2002 On the silicon spheroidization in Al–Si alloys *J. Light Met.* **2** 263
[11] Grinfeld M 2013 Thermodynamic models of phase transformations and failure waves *Wave Motion* **50** 1118
[12] Grinfeld M A 1991 *Thermodynamic Methods in the Theory of Heterogeneous Substances* (London: Longman)
[13] Buravova S N and Petrov E V 2018 Acceleration of mass transfer under dynamic loading *Russian Journal of Physical Chemistry B* **12** 120
[14] Djahanbakhsh M, Lojkowski W, Bürkle G, Ivanisenko Yu V, Valiev R Z and Fecht H J 2001 Nanostructure formation and mechanical alloying in the wheel/rail contact area of high speed trains in comparison with other synthesis routes *Mater. Sci. Forum* **360-362** 175
[15] Gromov V E, Yuriev A A, Ivanov Yu F and Glezer A M 2017 Defect substructure change in 100-m differentially hardened rails in long-term operation *Mater. Lett.* **209** 224
[16] Konovalov S, Chen X, Sarychev V, Nevskii S, Gromov V and Trtica M 2017 Mathematical modeling of the concentrated energy flow effect on metallic materials *Metals* **7** 1
[17] Sarychev V D, Khaimzon B B and Nevskii S A 2016 Solution of niobium in iron during arc surfacing *Steel in Translation* **46** 563
[18] Liu X *et al* 2018 Heat-treatment induced defect formation in $\alpha$-Al matrix in Sr-modified eutectic Al–Si alloy *J. Alloys Compd.* **730** 208
[19] Sheng Y *et al* 2018 Application of high-density electropulsing to improve the performance of metallic materials: mechanisms, microstructure and properties *Materials* **11** 185
[20] Kang N, Coddet P, Chen C, Wang Y, Liao H and Christian C 2016 Microstructure and wear behavior of *in situ* hypereutectic Al–high Si alloys produced by selective laser melting *Mater. Des.* **99** 120
[21] Brener E A, Weikamp M, Spatschek R, Bar-Sinai Y and Bouchbinder E 2016 Dynamic instabilities of frictional sliding at a bimaterial interface *J. Mech. Phys. Solids* **89** 149
[22] Michael A, Shiqing X, Brener Efim A, Yehuda B-Z and Eran B 2017 Nonmonotonicity of the frictional bimaterial effect *Journal of Geophysical Research: Solid Earth* **122** 8270
[23] Sarychev V, Nevskii S, Konovalov S, Granovskii A, Ivanov Y and Gromov V 2019 Model of nanostructure formation in Al–Si alloy at electron beam treatment *Mater. Res. Express* **6** 026540
[24] Lavrentiev M A and Yu I A 1949 Dynamic forms of loss of stability of elastic systems (in Russian) *Dokl. Phys.* **5** 778
[25] Belyaev A K, Morozov N F, Tovstik P E and Tovstik T P 2016 *Int. J. Eng. Sci.* **98** 92
[26] Kienzler R (ed) 2004 *Theories of Plates and Shells* (Berlin: Springer) (https://doi.org/10.1007/978-3-540-39905-6)
[27] Eslami M R, Hetnarski R B, Ignaczak J, Noda N, Sumi N and Tanigawa Y 2013 *Theory of Elasticity and Thermal Stresses: Explanations, Problems and Solutions* (Berlin: Springer) 978-9400799318 (https://doi.org/10.1007/978-94-007-6356-2)
[28] Forbes Lawrence K 2011 A cylindrical Rayleigh–Taylor instability: radial outflow from pipes or stars *J. Eng. Math.* **70** 205
[29] Rishi A, Kumar A M and Agrawal G S 2012 Viscous potential flow analysis of Rayleigh–Taylor instability of cylindrical interface *Applied Mechanics and Materials* **110-116** 769